

Spatiotemporal and Wavenumber Resolved Bicoherence at the Low to High Confinement Transition in the TJ-II Stellarator

B.Ph. van Milligen¹, T. Estrada¹, C. Hidalgo¹, T. Happel², E. Ascasíbar¹

¹*Asociación EURATOM-CIEMAT para Fusión, Avda. Complutense 40, 28040 Madrid, Spain and*

²*Max Planck Institut für Plasmaphysik, Association Euratom-IPP, 85748 Garching, Germany*

(Dated: February 1, 2013)

Plasma turbulence is studied using Doppler reflectometry at the TJ-II stellarator. By scanning the tilt angle of the probing beam, different values of the perpendicular wave numbers are probed at the reflection layer. In this way, the interaction between zonal flows and turbulence is reported with (a) spatial, (b) temporal, and (c) wavenumber resolution for the first time in any magnetic confinement fusion device.

We report measurements of the bicoherence across the Low to High (L–H) confinement transition at TJ-II. We examine both fast transitions and slow transitions characterized by an intermediate (I) phase. The bicoherence, understood to reflect the non-linear coupling between the perpendicular velocity (zonal flow) and turbulence amplitude, is significantly enhanced in a time window of several tens of ms around the time of the L–H transition. It is found to peak at a specific radial position (slightly inward from the radial electric field shear layer in H mode), and is associated with a specific perpendicular wave number ($k_{\perp} \simeq 6 - 12 \text{ cm}^{-1}$). In all cases, the bicoherence is due to the interaction between high frequencies and a rather low frequency, as expected for a zonal flow.

The spontaneous transition to the High confinement regime in fusion plasmas is a topic of great interest, due to its potential advantages for the design of a fusion reactor and the complex nonlinear physics involved. At the TJ-II stellarator, the transition from Low to High confinement (L–H) is “soft” in the sense that the confinement improvement factor is small, and yet it possesses the typical features of any L–H transition (rapid drop of H_{α} emission, reduction of fluctuation amplitudes, formation of a sheared flow layer, ELM-like bursts) [1, 2].

A common explanation for the L–H transition involves the generation of a zonal flow in a narrow radial region of the plasma near its edge. The zonal flow would be driven by turbulence via the Reynolds Stress mechanism in a strong pressure gradient region. The growth of the (fluctuating) zonal flow then leads to the suppression of turbulence, creating a transport barrier, and the subsequent establishment of a steady state sheared flow with associated radial electric field that maintains the barrier [3–5]. The detailed observation of this sequence of events is a challenge.

Due to the temporal and spatial scales involved in the L–H transition physics, specific experimental techniques are required to investigate the turbulence and flow dynamics [2]. At TJ-II, a two-channel Doppler reflectometer is available, allowing the simultaneous measurement of the perpendicular plasma velocity and density fluctuations at two radial positions, with good spatial and temporal resolution. In addition, the Doppler reflectometer offers the possibility to probe different turbulence scales (wave vectors) by steering the probing beam [6, 7].

Experimental setup – The TJ-II vacuum magnetic geometry is completely determined by the currents flowing in four external coil sets. At TJ-II, the normalized pressure $\langle\beta\rangle$ is generally low, even in discharges with Neu-

tral Beam Injection (NBI), and currents flowing inside the plasma are generally quite small (unless explicitly driven), so that the actual magnetic configuration and the rotational transform $\iota/2\pi$ are typically rather close to the vacuum magnetic configuration [8]. Here we focus on two magnetic configurations having $\iota(a)/2\pi = 1.630$ and 1.553.

The experiments have been carried out in pure NBI heated plasmas (line averaged plasma density $\langle n_e \rangle = 2 - 4 \times 10^{19} \text{ m}^{-3}$, central electron temperature $T_e = 300 - 400 \text{ eV}$). The NBI input heating power is kept constant at about 500 kW during the discharge but the fraction of NBI absorbed power – taking into account shine through, CX and ion losses, as estimated using a simulation code – increases from 55 to 70% as the plasma density rises.

In this work, we consider two different L–H transition scenarios. Standard or *fast* L–H transitions are observed in the magnetic configuration having $\iota(a)/2\pi = 1.630$ [6], while *slow* transitions are observed in the configuration having $\iota(a)/2\pi = 1.553$ and a low order rational (3/2) at $\rho = r/a \simeq 0.72$. In the latter configuration, the so-called intermediate phase (I), characterized by a predator-prey type interaction between turbulence and flows, appears between the L and H phases [9–11], which has also been seen in models [12, 13] and on other devices [14, 15]. In both scenarios, spatiotemporal and scale resolved Doppler reflectometry measurements were performed in series of repetitive discharges [6, 7].

Doppler reflectometry – In Doppler reflectometry, a finite tilt angle is purposely introduced between the incident probing beam and the normal to the reflecting cut-off layer, and the Bragg back-scattered signal is measured [16]. The amplitude of the recorded signal, A , is a measure of the intensity of the density fluctuations, \tilde{n} . By scanning the tilt angle of the probing beam, different

perpendicular wave numbers are probed, thus allowing scale-resolved turbulence measurements. Furthermore, as the plasma rotates in the reflecting plane (flux surface), the scattered signal experiences a Doppler shift. The size of this shift is directly proportional to the rotation velocity of the plasma turbulence perpendicular to the magnetic field lines, v_\perp , and therefore to the plasma background $E \times B$ velocity, provided the latter dominates over the phase velocity of density fluctuations (cf. [2]). The Doppler reflectometer signals, sampled at 10 MHz, allow determining \tilde{n} and v_\perp with high temporal and spatial resolution.

The relation between zonal flow growth, involving an interaction between high frequencies associated with drift wave turbulence and low frequencies associated with the zonal flow, and the cross bispectrum was elucidated in [17]. Probing zonal flow dynamics therefore requires measuring the cross bispectrum between the radial and poloidal $E \times B$ velocities of high-frequency drift waves and the low-frequency zonal flow. An early attempt at observing the bicoherence across the L–H transition was made at DIII-D [18]. As such measurements are quite difficult to perform in the plasma interior, the bicoherence is often calculated using density fluctuations only, which complicates the interpretation of the results. However, Doppler reflectometry allows the measurement of the turbulence fluctuation amplitude \tilde{n} as well as the fluctuating perpendicular flow \tilde{v}_\perp , both with good temporal and spatial resolution, making the two main quantities involved in zonal flow dynamics accessible experimentally. In this work, we consider the complex amplitude Doppler reflectometry signal, $Ae^{i\phi} = (A \cos \phi, A \sin \phi)$, which contains information of both the perpendicular flow, $\tilde{v}_\perp = d\tilde{\phi}/dt$, and the density turbulence, $\tilde{n} \propto \tilde{A}$.

Bicoherence analysis – The cross bicoherence of two signals $f(t)$ and $g(t)$ is defined as [19]

$$b_{fg}^2(\omega_1, \omega_2) = \frac{\langle |\hat{f}(\omega_1)\hat{f}(\omega_2)\hat{g}^*(\omega_1 + \omega_2)|^2 \rangle}{\langle |\hat{f}(\omega_1)|^2 \rangle \langle |\hat{g}(\omega_1 + \omega_2)|^2 \rangle},$$

where $\hat{f}(\omega)$ is the Fourier transform of $f(t)$, a star indicates the complex conjugate, and the angular brackets refer to an average over equivalent realizations. In practice, the equivalent realizations are successive time sections, assuming the system is in steady state. The value of b^2 is bounded between 0 and 1, so that a high value indicates wave-wave coupling between the two base frequencies ω_1 and ω_2 and their sum frequency, $\omega_1 + \omega_2$. The auto-bicoherence is $b_f^2 = b_{ff}^2$.

We also report the “summed bicoherence”, defined as $b_{\text{sum}}^2(\omega) = \langle b^2(\omega_1, \omega_2) \rangle_{\omega_1 + \omega_2 = \omega}$, and the “total bicoherence”, defined as $b_{\text{total}}^2 = \langle b^2(\omega_1, \omega_2) \rangle_{\omega_1, \omega_2}$. To judge the relevance of a bicoherence value, it is compared to the expectation value of the bicoherence under the assumption that the signal is uncorrelated random noise.

Computing the auto-bicoherence for the complex

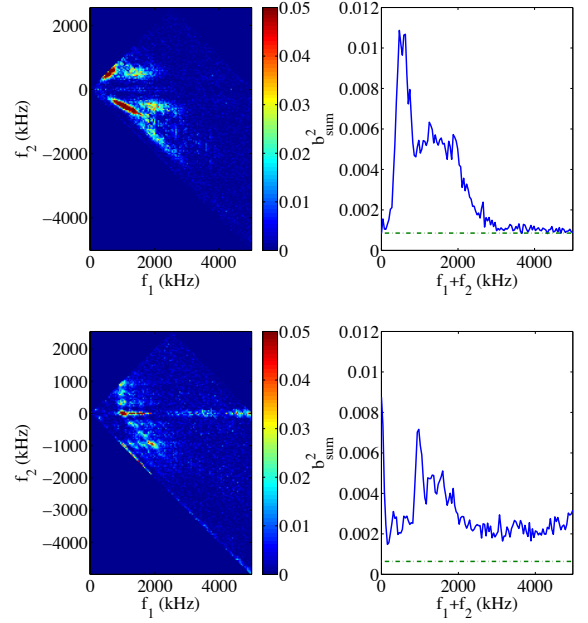


FIG. 1: Discharge 22277. Configuration with $\iota(a)/2\pi = 1.704$. Top: Mean auto-bicoherence and mean summed auto-bicoherence of complex Doppler reflectometry channel 1. Bottom: Cross bicoherence between \tilde{v}_\perp and \tilde{n} (Doppler reflectometry channel 1) during the L–H transition ($1100 < t < 1130$ ms, $t_{L-H} = 1116$ ms). The dashed line indicates the noise level.

Doppler reflectometer data around the time of the L–H transition, one typically obtains results such as those shown in Fig. 1. The auto-bicoherence is very significant, as the value is some two orders of magnitude above the noise level. The auto-bicoherence is concentrated along the line $f_2 \simeq -f_1/2$ (the ‘first harmonics’ line), $f_2 \simeq f_1$ (interaction with a very small difference frequency), and also at $f_2 \simeq 0$. These are indications that high frequencies f_a, f_b of the order of 1–2 MHz are interacting via a very small difference frequency $f_c = f_a - f_b$ (or harmonics $f_c = 2f_a - f_b$) such that $|f_c| \ll |f_a|, |f_b|$. Frequencies above 1 MHz are not commonly observed in this context due to technical limitations; however, note that similar results were obtained at DIII-D [18].

To facilitate the interpretation of the auto-bicoherence, Fig. 1 also shows the cross bicoherence between \tilde{v}_\perp and \tilde{n} for the same discharge. Here, significant coupling is limited mainly to the lines $f_2 \simeq 0$ and $f_2 \simeq \pm f_1$, indicating an interaction between two very similar frequencies f_a, f_b , interacting via a very small difference frequency $f_c = f_a - f_b$ such that $|f_c| \ll |f_a|, |f_b|$, while harmonics are weak. This is in fact what one would expect for the interaction between a zonal flow and turbulence [17, 20]. The small frequency of the triplet is at or below the frequency resolution (50 kHz), whereas the two high frequencies are in the range from 1 to 2 MHz. The fact

that the cross bicoherence graph shows linear structures, while the auto-bicoherence exhibits additional harmonic structures, is a clear indication that the physical interaction primarily involves \tilde{v}_\perp and \tilde{n} . Although the cross bicoherence between \tilde{v}_\perp and \tilde{n} is easier to interpret, the auto-bicoherence of the complex Doppler reflectometry signal (containing the same information) is easier to compute, not affected by the numerical errors inherent in the velocity calculation, and yields a larger signal to noise ratio in the total bicoherence value. Therefore, we will use the latter as a generic proxy to study the spatiotemporal evolution of the total bicoherence.

The fast L–H transition – To study the radial and temporal behavior of the bicoherence across the fast L–H transition, we have analyzed a series of 25 discharges in the same magnetic configuration ($\iota(a)/2\pi = 1.630$). See Ref. [6] for more details about this series of discharges. The Doppler reflectometer probing frequency and tilt angle were varied on a shot to shot basis, and correspondingly the radial position of the reflecting layer and the wave number k_\perp . Fig. 2a indicates the evolution of the density profile across the L–H transition. Due to the evolving profile, both the position of the reflecting layer and the wavenumber change as a function of time across the transition [6]. The measured channel locations and wave numbers are shown in Fig. 2b. Note that k_\perp varies by less than 5% between the L and H phases (matching black and red dots). The ρ and k_\perp values indicated on the axes of Figs. 2c–e correspond to the situation in H-mode. Note that ρ is a vacuum flux surface label; the actual confinement radius is somewhat less than $\rho = 1$ [21]. The temporal resolution of the bicoherence calculation is 2 ms.

Figs. 2c–e show the values of the auto-bicoherence $b^2(k_\perp, \rho, \Delta t)$, averaged over k_\perp , ρ , and Δt , respectively. It is seen that the bicoherence appears $\sim 20 - 30$ ms before the L–H transition at a specific radius ($\rho \lesssim 0.8$) and that specific perpendicular wave numbers are involved ($k_\perp \simeq 8 - 11 \text{ cm}^{-1}$). The bicoherence persists until about $10 - 20$ ms after the L–H transition. Similar behavior is observed across a wide range of magnetic configurations, showing that the phenomena are not associated with any specific rational surface.

It should be noted that turbulence is reduced at all scales, but most in intermediate scales, $k_\perp \simeq 7 - 11 \text{ cm}^{-1}$, as reported in earlier work [6]. After the transition, the radial electric field shear layer is located at $\rho \sim 0.83$, somewhat outward from the position of the maximum observed bicoherence values.

The slow L–I–H transition – Fig. 3 shows the auto-bicoherence for a different series of discharges in the configuration with $\iota(a)/2\pi = 1.553$. The elaboration of this figure is equivalent to that of Fig. 2. The mean line average density at the transition is about 50% lower than with the previous configuration. Another difference with the previous result is that in these discharges, the tran-

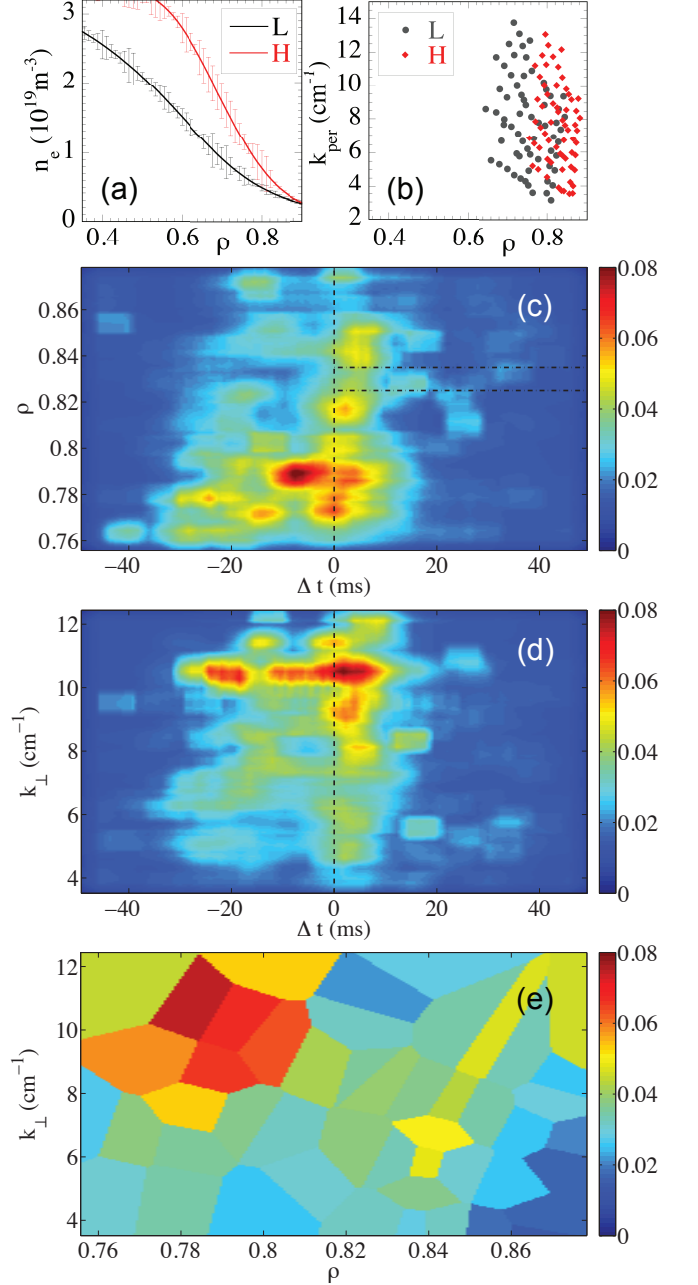


FIG. 2: Series of 25 discharges in the configuration with $\iota(a)/2\pi = 1.630$. Total auto-bicoherence of complex Doppler reflectometry data. (a) Density profiles in the L and H phases. (b) Position ρ and k_\perp of the measurement channels in the L and H phases. (c) Mean auto-bicoherence vs. time and normalized radius, ρ . (d) Mean auto-bicoherence vs. time and k_\perp . (e) Mean auto-bicoherence vs. ρ and k_\perp (averaged over $-10 \leq \Delta t \leq 10$ ms). Radii and k_\perp values of Figs. (c) – (e) correspond to the H phase. The vertical dashed line indicates the L–H transition; the horizontal dashed lines indicate the approximate position of the E_r shear layer in the H phase. The statistical error level is about 0.006.

sition at $\Delta t = 0$ is not into the H-mode, but rather into the intermediate (I) phase between the L-mode ($\Delta t < 0$) and the H-mode (starting much later). We conjecture that this situation is due to a weaker zonal flow, incapable of producing the final transition into the H phase. This would be consistent with the observation of the predator-prey relation between turbulence and flows, associated with wave numbers in the range $k_{\perp} \simeq 6 - 12 \text{ cm}^{-1}$, as confirmed by spectral analysis [7].

The location of the auto-bicoherence peak appears to be somewhat further inward than in the previous section ($\rho < 0.76$).

Discussion and conclusions – In this work, we have used Doppler reflectometry measurements to show how the bicoherence evolves across the L–H transition at TJ-II. It is the first time that turbulent fluctuation amplitudes and perpendicular (zonal) flow oscillations and their non-linear interactions have been observed simultaneously in the region of the plasma where the transport barrier of the L–H transition forms. The observation of the bicoherence does not appear to depend very sensitively on the magnetic configuration. A surprisingly clear picture emerges that is consistent with established ideas about the interaction between zonal flows and turbulence [22] in the important formation phase of the H-mode transport barrier.

In the case of the fast L–H transition, we have shown that the auto-bicoherence of the Doppler reflectometer signal is significant in a time window with a length of several tens of ms around the L–H transition time [18], at a particular radial position ($\rho \lesssim 0.8$, inward from the radial electric field shear layer in H mode), and that a specific range of perpendicular wave numbers is involved ($k_{\perp} \simeq 8 - 11 \text{ cm}^{-1}$). Here, $\rho_s = \sqrt{2m_i T_e}/eB = 0.1 - 0.2 \text{ cm}$, so that this range corresponds to $k_{\perp} \rho_s = 0.8 - 2$.

A similar analysis in another set of discharges corresponding to a different magnetic configuration, in which the transition was characterized by an intermediate phase separating the L and H phases, the bicoherence appeared only after the L–I transition was made, and lasted several tens of ms afterward into the I phase. The perpendicular wave numbers involved ($k_{\perp} \simeq 6 - 12 \text{ cm}^{-1}$) were very similar to the previous case, while the radial location of the bicoherence peak was somewhat further inward ($\rho < 0.76$).

In both cases, the auto-bicoherence was due to high frequencies (of the order of 1–2 MHz) interacting with rather low frequencies ($< 50 \text{ kHz}$), as expected for a zonal flow [13]. With the available data, it is not feasible to clearly resolve the low frequency component.

Putting these results into context, we note that this is the first time wave number resolved bicoherence during L–H transitions is reported. This important result indicates which spatial scales are important in the zonal flow coupling producing the L–H transition.

Acknowledgements – The authors would like to ex-

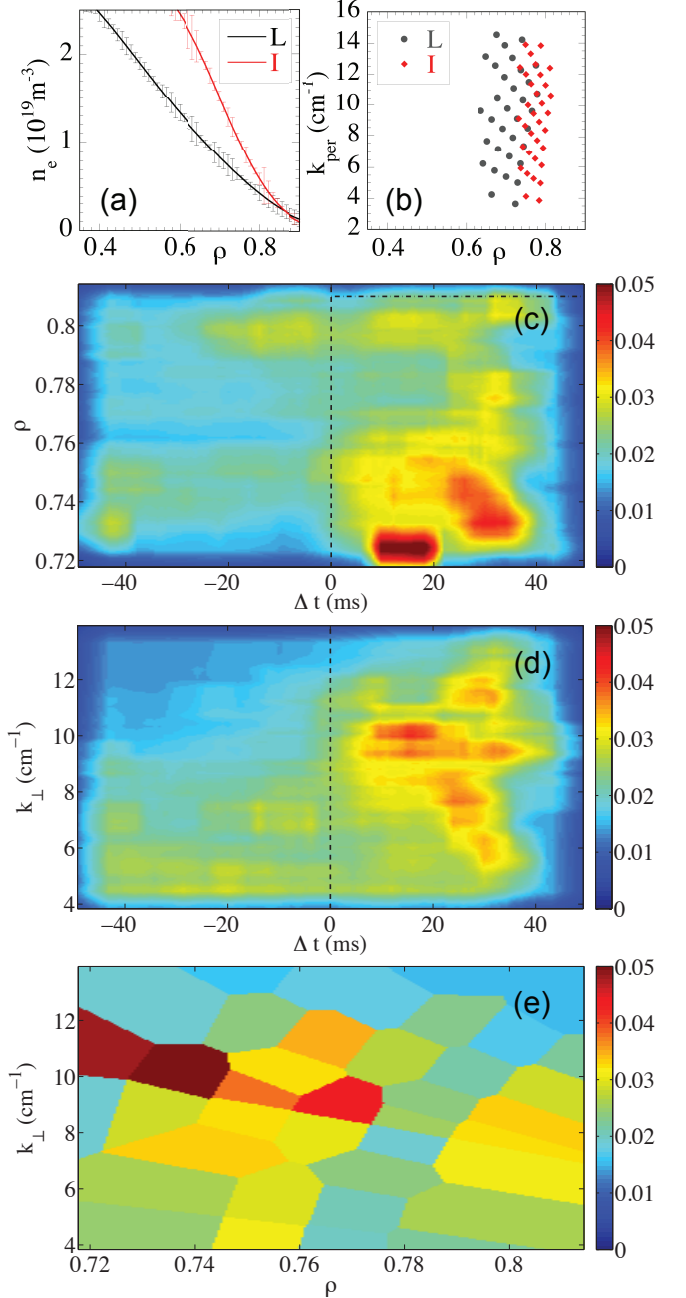


FIG. 3: Series of 26 discharges in the configuration with $\iota(a)/2\pi = 1.553$. Total auto-bicoherence of complex Doppler reflectometry data. (a) Density profiles in the L and I phases. (b) Position ρ and k_{\perp} of the measurement channels in the L and I phases. (c) Mean auto-bicoherence vs. time and normalized radius, ρ . (d) Mean auto-bicoherence vs. time and k_{\perp} . (e) Mean auto-bicoherence vs. ρ and k_{\perp} (averaged over $0 \leq \Delta t \leq 20 \text{ ms}$). Radii and k_{\perp} values of Figs. (c) – (e) correspond to the I phase. The vertical dashed line indicates the L–I transition; the horizontal dashed line indicates the approximate position of the E_r shear layer in the I phase. The statistical error level is about 0.006.

press their gratitude for continued support by the TJ-II team. Research sponsored in part by DGICYT of Spain under project Nrs. ENE2009-07247 and ENE2010-18409.

-
- [1] J. Sánchez, M. Acedo, A. Alonso, J. Alonso, P. Alvarez, E. Ascasíbar, A. Baciero, R. Balbín, L. Barrera, E. Blanco, et al., *Nucl. Fusion* **49**, 104018 (2009).
 - [2] T. Estrada, T. Happel, L. Eliseev, D. López-Bruna, E. Ascasíbar, E. Blanco, L. Cupido, J. Fontdecaba, C. Hidalgo, R. Jiménez-Gómez, et al., *Plasma Phys. Control. Fusion* **51**, 124015 (2009).
 - [3] K. Burrell, *Phys. Plasmas* **4**, 1499 (1997).
 - [4] P. Diamond, S.-I. Itoh, K. Itoh, and T. Hahm, *Plasma Phys. Control. Fusion* **47**, R35 (2005).
 - [5] F. Wagner, *Plasma Phys. Control. Fusion* **49**, B1 (2007).
 - [6] T. Happel, T. Estrada, E. Blanco, C. Hidalgo, G. Conway, U. Stroth, and the TJ-II Team, *Phys. Plasmas* **18**, 102302 (2011).
 - [7] T. Estrada, E. Ascasíbar, E. Blanco, A. Cappa, P. Diamond, T. Happel, C. Hidalgo, M. Liniers, B. van Milligen, I. Pastor, et al., *Plasma Phys. Control. Fusion* **54**, 124024 (2012).
 - [8] B. van Milligen, T. Estrada, E. Ascasíbar, D. Tafalla, D. López-Bruna, A. López-Fraguas, J. Jiménez, I. García-Cortés, A. Dinklage, R. Fischer, et al., *Rev. Sci. Instrum.* **82**, 073503 (2011).
 - [9] R. Colchin, B. Carreras, R. Maingi, L. Baylor, T. Jernigan, M. Schaffer, T. Carlstrom, N. Brooks, C. Greenfield, P. Gohil, et al., *Nucl. Fusion* **42**, 1134 (2002).
 - [10] T. Estrada, T. Happel, C. Hidalgo, E. Ascasíbar, and E. Blanco, *Eur. Phys. Lett.* **92**, 35001 (2010).
 - [11] T. Estrada, C. Hidalgo, T. Happel, and P. Diamond, *Phys. Rev. Lett.* **107**, 245004 (2011).
 - [12] E.-J. Kim and P. Diamond, *Phys. Plasmas* **10**, 1698 (2003).
 - [13] K. Miki, P. Diamond, Ö. Gürcan, G. Tynan, T. Estrada, L. Schmitz, and G. Xu, *Phys. Plasmas* **19**, 092306 (2012).
 - [14] G. Conway, C. Angioni, F. Ryter, P. Sauter, J. Vicente, and the ASDEX Upgrade Team, *Phys. Rev. Lett.* **106**, 065001 (2011).
 - [15] L. Schmitz, L. Zeng, T. Rhodes, J. Hillesheim, E. Doyle, R. Groebner, W. Peebles, K. Burrell, and G. Wang, *Phys. Rev. Lett.* **108**, 155002 (2012).
 - [16] M. Hirsch, E. Holzhauer, J. Baldzuhn, B. Kurzan, and B. Scott, *Plasma Phys. Control. Fusion* **43**, 1641 (2001).
 - [17] P. Diamond, M. Rosenbluth, E. Sánchez, C. Hidalgo, B. van Milligen, T. Estrada, B. Brañas, M. Hirsch, H. Hartfuss, and B. Carreras, *Phys. Rev. Lett.* **84**, 4842 (2000).
 - [18] R. Moyer, G. Tynan, C. Holland, and M. Burin, *Phys. Rev. Lett.* **87**, 135001 (2001).
 - [19] Y. Kim and E. Powers, *Phys. Fluids* **21**, 1452 (1978).
 - [20] Y. Nagashima, K. Itoh, S.-I. Itoh, A. Fujisawa, K. Hoshino, Y. Takase, M. Yagi, A. Ejiri, K. Ida, K. Shinohara, et al., *Plasma Phys. Control. Fusion* **48**, S1 (2006).
 - [21] E. Ascasíbar, T. Estrada, F. Castejón, A. López-Fraguas, I. Pastor, J. Sánchez, U. Stroth, J. Qin, and TJ-II Team, *Nucl. Fusion* **45**, 276 (2005).
 - [22] A. Fujisawa, A. Shimizu, H. Nakano, S. Ohshima, K. Itoh, Y. Nagashima, S.-I. Itoh, H. Iguchi, Y. Yoshimura, T. Minami, et al., *Plasma Phys. Control. Fusion* **49**, 211 (2007).